HOKKAIDO UNIVERSITY

Title	Mechanical Properties of a 3 Dimensional-Printed Transparent Flexible Resin Used for Vascular Model Simulation Compared with Those of Porcine Arteries
Author(s)	Morita, Ryo; Nonoyama, Takayuki; Abo, Daisuke et al.
Citation	Journal of vascular and interventional radiology, 34(5), 871-878.e3 https://doi.org/10.1016/j.jvir.2023.01.008
Issue Date	2023-05
Doc URL	https://hdl.handle.net/2115/93050
Rights	© 2023. This manuscript version is made available under the CC-BY-NC-ND 4.0 license http://creativecommons.org/licenses/by-nc-nd/4.0/
Rights(URL)	https://creativecommons.org/licenses/by-nc-nd/4.0/
Type	journal article
File Information	HUSCAP JVIR 34(5) 871-878.e3.pdf

Hokkaido University Collection of Scholarly and Academic Papers : HUSCAP

Mechanical Properties of a 3 Dimensional–Printed Transparent Flexible Resin Used for Vascular Model Simulation Compared with Those of Porcine Arteries

Ryo Morita, M.D., Ph.D.[a], Takayuki Nonoyama, Ph.D.[b], Daisuke Abo, M.D., Ph.D.[a], Takeshi Soyama, M.D.Ph.D.[c], Fujima Noriyuki, M.D.Ph.D.[a], Tetsuaki Imai, M.D., Ph.D.[d], Hiroyuki Hamaguchi, RT[e], Takuto Kameda, RT[e], Osamu Sugita, Ph.D.[f], Bunya Takahashi, M.D.[a], Naoya Kinota, M.D.[a], Kohsuke Kudo, M.D., Ph.D.[g,h]

[a] Department of Diagnostic and Interventional Radiology, Hokkaido University Hospital, N-14, W-5, Kita-ku, Sapporo, Hokkaido 060-8648, Japan

[b] Faculty of Advanced Life Science, Hokkaido University, Kita-21, Nishi-11, Kita-ku, Sapporo 001-0021, Japan.

[c] Department of Diagnostic and Interventional Radiology, Kushiro City General Hospital, 1-12 Shunkodai, Kushiro, Hokkaido 085-0822, Japan

[d] Department of Neurosurgery, Hakodate Central General Hospital, 33-2 Honcho, Hakodate, Hokkaido 040-8585, Japan

[e] Department of Radiological Technology, Hokkaido University Hospital, N-14, W-5, Kita-ku, Sapporo, Hokkaido 060-8648, Japan

[f] Institute of Health Science Innovation for Medical Care, Clinical Development Division, Hokkaido University Hospital, N-14, W-5, Kita-ku, Sapporo, Hokkaido 060-8648, Japan

[g] Department of Diagnostic Imaging, Faculty of Medicine, Hokkaido University, N-15, W-7, Kita-ku, Sapporo, Hokkaido 060-8638, Japan

[h] Global Center for Biomedical Science and Engineering, Faculty of Medicine, Hokkaido University, N-14, W-5, Kita-ku, Sapporo, Hokkaido 060-8648, Japan

Corresponding author:

Ryo Morita

Department of Diagnostic and Interventional Radiology, Hokkaido University Hospital

N-14 W-5, Kita-ku, Sapporo, Hokkaido 060-8648, Japan

Tel: 81-11-706-7779

Fax: +81-11-706-7876

E-mail: ryo561201@me.com

Funding: This work was financially supported by funds from a Grant-in-Aid for Young Scientists (Start-up) 20K22862 from the Japan Society for Promotion of Science, and the Medical Image Lab for providing materials for this study.

Conflict of interest: This study was funded by the Medical Image Lab.

Word count: 3766

Informed consent: Written informed consent was obtained from the patients for publication of this report and any accompanying images.

Acknowledgements: This work was financially supported by funds from a Grant-in-Aid for Young Scientists (Start-up) 20K22862 from the Japan Society for Promotion of Science. The authors thank the ‘‘Highly accurate diagnostic and interventional radiology by materializing image data” financially supported by the Medical Image Lab for this study.

Laboratory Investigation: Preclinical (no human subjects)

- Laboratory (no live animals)

Type of Study: Comparative Study

Level of Evidence: Limited quality experience: observational or registry study with limited design and execution, systematic review or meta analysis of such limited studies

- The material was not presented at an SIR Annual Scientific Meeting.

Mechanical Properties of a 3 Dimensional–Printed Transparent Flexible Resin Used for Vascular Model Simulation Compared with Those of Porcine Arteries

Abstract

Purpose: To develop a vascular intervention simulation model that replicates the characteristics of a human patient, the mechanical properties of a three-dimensional (3D)-printed transparent flexible resin were compared with those of porcine arteries using the elastic modulus (*E*) and kinetic friction coefficient (μ_k).

Materials and Methods: Resin plates were created from transparent flexible resin using a 3D printer. Porcine artery plates were prepared by excising the aorta. *E*, adhesive strength of resin and arterial surface toward polyethylene plate, was measured with a tensile-compressive mechanical tester. The resin transparency was measured with an ultraviolet-visible light spectrometer. μ_k of the resin plate surface after applying silicone spray for 1–5 s and that of the artery were measured with a translational friction tester.

Results: *E* differed significantly between the arteries and resin plates at each curing time (0.20 ±0.04 vs. 8.53 ±2.37 MPa for a curing time of 1 min, $P<0.05$). The resin was stiffer than the arteries, regardless of the curing times. The visible light transmittance and adhesive strength of the resin decreased as the curing time increased. The adhesive strength of the artery was the lowest. μ_k of the silicone-coated resin surface created by applying silicone

for 2–3 s (thickness of the silicone layer: 1.6–2 μm) was comparable with that of the artery, indicating that the coating imparted a similar slippage to the resin as the living artery.

Conclusion: Transparent flexible resin is useful for creating a transparent and slippery vascular model for vascular intervention simulation.

Key words: preoperative simulation, patient-specific hollow vascular model, three-dimensional printer

Abbreviations: E = elastic modulus, IR = interventional radiology, MRI = magnetic resonance imaging, SLA = stereolithography, PE = polyethylene, PSHVMs = patient-specific hollow vascular models, 3D = three-dimensional, μ_k = kinetic frictional coefficient.

Introduction

Three-dimensional (3D) printing technology has enabled the rapid and easy production of patient-specific hollow vascular models (PSHVMs) (1, 2). PSHVMs have been applied in several areas, including abdominal vessels (2-4), for preoperative simulation, training, and educating residents and students in interventional radiology (IR) (5-8). Compared with standard vascular models (9) or virtual reality simulations (10), IR simulation of endovascular treatment with PSHVMs has greater clinical applicability (5, 11) as the vascular geometry of individual patients can be reproduced.

Vascular models are required to possess flexibility similar to that of the vascular tissue (elastic modulus [*E*]) and appropriate sliding that mimics the vascular lumen (surface friction).

E and the friction coefficient (μ_k) of a silicone vascular model have been studied (12-14). Although expensive due to the technically difficult and time-consuming process, "ready-made" silicone can be used to manufacture transparent, flexible vascular models with good sliding properties (9). Since printing complex hollow structures, such as vessels, directly with 3D printers using silicone was virtually impossible (15), combining the lost-wax technique to create hollow vessels using various materials was necessary(1).

Stereolithography (SLA) is a liquid-based layered modeling process based on the photo-polymerization of resin, where ultraviolet light is used to cure each layer slice-by-slice (16,

17). Currently, available commercial desktop SLA type 3D printers allow easy printing of an actual model of the individual patient (7, 18). PSHVMs have been manufactured using these desktop 3D printers at medical facilities, with the transparent and flexible of these models making them promising (18, 19). Thus creating a vascular model suitable for IR simulation for individual patients using a desktop 3D printer (Figure E1a) is possible.

The vascular models were manufactured using a transparent flexible material, Flexible 80A (Figure E1b), and would be useful in the field of IR (see Video 1).

This study aimed to develop a vascular intervention simulation model that replicates the characteristics of a human patient. We hypothesized that a tailored 3D-printed material, Flexible 80A, may be designed to mimic the arterial wall characteristics. To prove this hypothesis, the 3D-printed resins were compared with porcine arteries using indices, such as *E* and μ_k, and adhesive strength, in addition to basic resin characteristics, such as transparency.

Materials and Methods

Preparation of resin, and porcine artery plates

Flexible 80A (Formlabs, Somerville, MA, USA), a transparent flexible resin, was used to create thin resin plates with a 3D printer, Form 3L (Formlabs). Before 3D printing, thin rectangular or circular Standard Triangulated Language (STL) data was obtained using

Fusion 360 (Autodesk, San Rafael, CA, USA) to make the required size for the following tests. Subsequently, the data were evaluated for corruption by PreForm (Formlabs), and this software sent the data to the printer. The resin plates (Figure 1) were created without support materials using Form 3L. The designed resin plates were washed with isopropyl alcohol, dried, and cured with FormCure (Formlabs) for 1–10 min (curing times). The silicone spray (Shin-Etsu Chemical Co., Ltd, Tokyo, Japan) , which consisted of dimethyl silicone oil, was applied from a fixed distance of 15 cm from the resin plate to alter the frictional properties of the surface.

Porcine artery plates (Figure 1) were created by excising the abdominal aorta immediately postmortem (Sus scrofa domesticus, 6-month-old female pigs crossbred from three races: Landrace, Middle White and Berkshire). Approval of the institutional animal care and use committee protocol was not required for this study. The aorta was cut longitudinally around the attachment of the intercostal artery, flattened, cut to approximately the same size as the resin plates, and immersed in physiological saline (Otsuka Pharmaceutical Co, Ltd, Tokyo, Japan) to prevent tissue dehydration; care was taken not to damage the endothelium. Simple geometry, such as a flat plate, was employed to quantitatively evaluate mechanical properties since the actual geometry of arteries is very complicated with individual differences.

Tests for characterization of flexible 80A resin

・***Unidirectional tensile test.***——E (MPa) of the resin and porcine artery were measured with a tensile-compressive mechanical tester (Autograph AGX, Shimadzu, Japan). The curing times of the resin were 0, 1, 3, 5, and 10 min. The artery and resin plate were respectively 27.67±1.37 mm long, 14.92±1.65 mm wide, and 1.36±0.20 mm thick and 21.40±1.64 mm long, 15.04±0.09 mm wide, and 2.69±0.20 mm thick. The sheet sample was fixed by clamps connected to a 1 kN load cell, and the tensile test was performed at a velocity of 10 mm/min (Figure 2a). E was calculated from the initial linear slope at a strain of approximately 0.004–0.008 (pig), 0.001–0.004 (resin). The numbers of artery and resin samples used in the test were 6 and 7, respectively.

・***Ultraviolet-visible light (UV-Vis) absorption spectroscopy.*** ——The transparency of the resin was measured with the UV-Vis spectrometer (UV-1800, Shimadzu, Japan). The curing times of resin were 0, 1, 3, 5, and 10 min. The sample thickness was 3 mm. The transmittance (T, %) was measured from 200 to 900 nm.

・***Tack test.*** ——The adhesive strength (σ_A, kPa) and energy (Γ_A, MJ/m^2) of the resin surface (n=6) and artery surface (n=6) toward the polyethylene (PE) plate, the same material with the catheter tip, were measured with a tensile-compressive mechanical tester (Autograph AGX, Shimadzu, Japan) (Figure 2b). The curing times of the resin were 0, 1, and 10 min. The disc geometry of the samples of resin and artery was 15-mm diameter and 3-mm thickness, 1.76 (±0.08) mm, respectively. The disc was fixed to the bottom of the brass-hammer cylinder jig

connected to the 100 N load cell. The disc sample contacted the PE plate with 10 N normal force for 1 min and was then detached. σ_A and Γ_A corresponded to the maximum force and accumulative area of the load-displacement curve during the detachment.

Characterization of the silicone-coated resin

・***Friction test.*** ——The kinetic frictional coefficient (μ_k) of the resin and inner surface of the porcine artery contacting to alumina ball (φ=15 mm) was measured with a translational friction tester (Type14DR, Shinto Scientific, Japan) (20) (Figure E2a). The curing time of the resin was 3 min, and the silicone coating durations were 0, 1, 2, 3, 4, and 5 s. The test atmosphere were air and saline solution. The artery tube was cut longitudinally, and the specimen was fixed horizontally to the tailor-made bath (Figure E2b). The normal force, translational displacement, and test speed were 50 gf, 32 mm, and 1000 mm/min, respectively. μ_k was calculated from the plateau frictional force behind the peak force as the static friction. A total of 12 resin plates and one artery plate were used for each silicone application time (0-5s) in each condition (air/saline). The average and standard deviation were obtained from the data of 10 cycles.

・***3D laser microscopy.*** ——The thickness of the silicone-coated layer on the resin plate was measured by a 3D laser microscope (VK-9710 KEYENCE, Osaka, Japan). Half of the resin plate was covered with low-sticky tape and then silicone-coated for 1, 2, 3, 4, and 5 s. The

tape was removed just before the imaging. The height of the image at the coating boundary was acquired at a laser wavelength of 408 nm. One resin plate was used for each silicone coating time(1-5s). For each time, the height of 9 locations were measured for one plate by 3D laser microscopy.

Statistical analyses

The normality of the continuous variables was assessed using the Shapiro–Wilk test. Continuous variables were compared using one-way analysis of variance (ANOVA). Dunnett's and Tukey's tests were used for post-hoc analysis when ANOVA gave a positive result. Dunnett's and Tukey's tests were performed on all quantitative data with BellCurve for Excel software (Social Survey Research Information Co., Ltd.). $P<0.05$ was considered statistically significant. Multiple comparisons (Dunnett's and Tukey's tests) were performed with Bonferroni correction.

Unidirectional tensile test: Comparison among five resin groups (curing times of 0, 1, 3, 5, and 10 min) was performed with one-way ANOVA and Tukey's test. In addition, Dunnett's test was performed with the five resin groups, using the porcine artery group as the control.

Tack test: Comparison among three resin groups (curing times of 0, 1, and 10 min,) and the artery group was performed using Tukey's test.

Friction test: The porcine artery group was used as the control. Dunnett's test was performed with resin groups with silicone-coating durations of 0, 1, 2, 3, 4, and 5 s in air or saline,.

3D laser microscopy: Comparison of the thickness of the silicone coating among the resin groups with various silicone coating durations (1, 2, 3, 4, and 5 s) was performed using Tukey’s test.

Results

General characteristics of Flexible 80A resin

・***Unidirectional tensile test.*** ——Figure 3a shows the results of the unidirectional tensile test. *E* of the porcine artery was 0.20 (±0.04) MPa. *E* of the resin with curing times of 0, 1, 3, 5, and 10 min was 5.50 (±1.15), 8.53 (±2.37), 8.63 (±1.12), 9.50 (±1.43), and 8.89 (±1.45) MPa, respectively. Dunnett's test showed significant differences between the porcine arteries and resin plates at each curing time ($P<0.05$). Multiple comparisons were performed using Tukey’s test for the resin. A significant difference in *E* was observed between the 0-min and 5- and 10-min curing time groups ($P<0.05$); however, no significant differences were identified in the comparisons of the other combinations. The resin plates were stiffer than porcine arteries regardless of the curing times.

・***UV-Vis absorption spectroscopy.*** —— The resin materials were impermeable to light with wavelengths below 400 nm. Figure E3 shows the visible light transmittance (*T*, %, 400–700 nm) of resin with curing times of 0, 1, 3, 5, and 10 min, indicating that the transmission of visible light decreases in proportion to the curing times above 400 nm.

・***Tack test.***——Figure 3b shows the results of the Tack test. The adhesive strength and energy of the uncured resin were higher than those of the cured resin ($P<0.05$). The adhesive strength and energy of the 10-min cured resin were lower than those of the 1-min cured resin; the adhesive strength of the artery was the lowest. The artery had a higher adhesive energy than the 10-min cured resin because of the deformation of the arterial tissue during the peeling process. Significant differences were observed between all groups ($P<0.05$) , except for adhesive energy between the artery and 10-min resin groups. These data demonstrate that curing the resin reduces the adhesive strength.

・***Setting of curing time of resin plate.***——The curing time was set to 1 min to attain the required transparency and adhesiveness of the resin plate.

Characteristics of silicone-coated resin

・***Friction test.*** ——Figure 4 shows the results of the friction test. μ_k of the inner surface of the porcine artery in saline solution was 0.0547 (±0.0253). μ_k of the resin plates with silicone coating durations of 2 and 3 s in air was 0.0604 (±0.0212), and 0.0596 (±0.0079),

respectively; the corresponding values in saline solution were 0.0378 (±0.0186), and 0.0340 (±0.0072), respectively. There were no significant differences in μ_k between the porcine artery and silicone-coated resins with coating durations of 2 and 3 s in the air and between the porcine artery and silicone-coated resin with coating durations of 2, 3, and 4 s in the saline solution. Therefore, the silicone-coated resin surfaces created by spraying silicone for 2 and 3 s in air and saline solution possessed μ_k that was comparable with that of the porcine artery.

・***3D laser microscopy.*** ——Figure E4a shows the thickness of the silicone layer on the resin. The thickness increased significantly with increased spraying time ($P<0.05$); however, it plateaued at 4 and 5 s. Figure E4b shows the relationship between μ_k and the thickness of the silicone coating on the resin. The thickness of the silicone layer (1.6–2 μm) at 2 and 3 s exhibited similar μ_k as the porcine artery.The frictional force increased by increasing the thickness of the silicone coating over about 2.4 μm.

・Table 1 summarizes these results.

Discussion

This study shows that it is possible to create transparent slippery vascular models using Flexible 80A by setting the curing time to 1 min and applying silicone spray for 2–3 s (thickness of the silicone layer: 1.6–2 μm). This material is sufficiently flexible for IR

simulations and feasible in terms of creating vascular models for individual patient using a desktop 3D printer.

Creating a hollow vascular model directly from a 3D printer without internal supports was technically difficult (4, 11, 16). With increased technological developments, flexible hollow vascular models have been printed directly from a 3D printer; however, most flexible models are not transparent, and the catheters are not visible, thereby necessitating the use of fluoroscopy (3, 5). In contrast, Flexible80A （75–95% acrylate monomer, 3–6% urethane dimethacrylate based resin) is a light-cured resin classified as an elastic and transparent resin (18). The advantages of using transparent, flexible resin for creating ideal vascular models have been reported (18, 19), such as the catheter being visible without fluoroscopy (Figures E1 and Video 1).

The transparency decreased, and the adhesive strength reduced with increased curing time (Figure 3b/E3). It is best to use uncured resin plates in terms of transparency. However, the uncured resin showed high adhesiveness in the adhesion test, which was presumed to be due to the residual uncured resin on the plate surface. The high adhesive strength is believed to reduce the sliding of the luminal surface of the vascular model. Therefore, considering both transparency and adhesiveness, the curing time was set to 1 min.

The results of the friction test indicate that the friction property of the porcine artery is almost comparable with that of the appropriate silicone-coated resin. A previous friction test

using porcine arteries reported a μ_k of 0.0384 (± 0.0100) (20), which is close to the value of 0.0547 (± 0.0253) reported in our study. The reduction in the friction of silicone-coated resin could be due to the silicone coating filling the surface irregularities and making the surface smooth (Figure E4a). μ_k of the luminal surface of the silicone vascular model reportedly reduced by up to 55% with the use of liquid silicone rubber coating (21). The frictional force increased by increasing the thickness of the silicone coating over 2.4 μm (Fig. E4b), possibly due to the fluid resistance from the deformation of the silicone layer, resulting in an increase in the frictional force due to the thicker coating.

Few reports have stated that the sliding can be improved with water flow by connecting a peristaltic fluid pump (7, 18, 19); however, the preparation is complicated, and an expensive peristaltic fluid pump is required. In contrast, this study revealed that the simple method of applying silicone coating of appropriate thickness could provide vascular models with slippage similar to that of living arteries in saline and air atmospheres. Thus, silicone coating could enable IR simulations without a flow device. In addition, materials other than Flexible 80A could be used to create models with similar slippage and the same silicone application.

Our study revealed that the resin plates were stiffer than the porcine arteries [0.20 (±0.04) MPa] regardless of the curing time. *E* of a healthy human arterial wall is reported to be 1.48 (±0.24) MPa (22). Although aging and progression of atherosclerosis cause stiffening of the artery wall, it does not exceed 5 MPa (22, 23), suggesting that the stiffness of a resin with a

curing time of 0 min [5.50 (±1.15) MPa] is slightly higher than that of the human arterial wall. Successful treatment of a case with high-flow renal arteriovenous fistula after simulation using a vascular model made of Flexible 80A has been reported (8). In addition, as shown in Fig. E1b, this material is sufficiently flexible to deform when a stiff wire or thick catheter is inserted, indicating that Flexible 80A has sufficient flexibility to be used in the simulation. In addition, localized flexural tortuous vessel models with made of materials softer than Flexible 80A with *E* of 1–2 MPa, which is closer to that of the normal human artery, have fractured during device insertion (24).

A vascular models created with Flexible 80A resin lacks surrounding tissues. The loss of the potential effect of the surrounding tissue should be considered. Intracranial vessels are substantially less deformable as they are encased in bone. In contrast, extracranial vessels are deformable and covered by surrounding soft tissue, such as fat and muscles, which maintain their shape. This vascular model has a high *E* and is substantially less deformable compared with the vessels. Therefore, this model does not require surrounding material. In contrast, a vascular model created with a softer material similar to the artery may require surrounding materials, such as a gel (25). The stiffness of this model, present without surrounding support, is advantageous in a practice model in terms of understanding the positioning of the vessels.

Creating a custom model for each patient is expensive and time-consuming. Therefore, an expert may use this model, albeit rarely, only in anatomically challenging cases. However, if these models are available easily by storing several vascular models created based on the computed tomography images of the patient, custom models can be used to train students and trainees, as well as for preoperative planning by experts.

This study has some limitations. First, porcine arteries from healthy pigs were used as controls, instead of human arteries from patients with atherosclerosis. Second, we did not evaluate materials other than resin for comparison. Third, due to the differences in *E* between the model and arteries, there may be a need to investigate how this affects the physician's use of the model.

In conclusion, Flexible 80A resin with silicone coating may a promising material for developing a vascular intervention simulation model that replicates the characteristics of a human patient.

References

[1] Knox K, Kerber CW, Singel SA, et al. Stereolithographic vascular replicas from CT scans: choosing treatment strategies, teaching, and research from live patient scan data. AJNR Am J Neuroradiol 2005; 26:1428-31.
[2] Itagaki MW. Using 3D printed models for planning and guidance during endovascular intervention: a technical advance. Diagn Interv Radiol 2015; 21:338-41. DOI: 10.5152/dir.2015.14469
[3] Mashiko T, Otani K, Kawano R, et al. Development of three-dimensional hollow elastic model for cerebral aneurysm clipping simulation enabling rapid and low cost prototyping. World Neurosurg 2015; 83:351-61. DOI: 10.1016/j.wneu.2013.10.032

[4] Takao H, Amemiya S, Shibata E, et al. 3D Printing of Preoperative Simulation Models of a Splenic Artery Aneurysm: Precision and Accuracy. Acad Radiol 2017; 24:650-3. DOI: 10.1016/j.acra.2016.12.015
[5] Goudie C, Kinnin J, Bartellas M, et al. The Use of 3D Printed Vasculature for Simulation-based Medical Education Within Interventional Radiology. Cureus 2019; 11:e4381. DOI: 10.7759/cureus.4381
[6] Tenewitz C, Le RT, Hernandez M, et al. Systematic review of three-dimensional printing for simulation training of interventional radiology trainees. 3D Print Med 2021; 7:10. DOI: 10.1186/s41205-021-00102-y
[7] Torres IO, De Luccia N. A simulator for training in endovascular aneurysm repair: The use of three dimensional printers. Eur J Vasc Endovasc Surg 2017; 54:247-53. DOI: 10.1016/j.ejvs.2017.05.011
[8] Morita R, Abo D, Soyama T, et al. Usefulness of preoperative simulation with patient-specific hollow vascular models for high-flow renal arteriovenous fistula embolization using a preloading coil-in-plug technique. Radiology Case Reports 2022; 17:3578-86. DOI: 10.1016/j.radcr.2022.07.028
[9] Yamagami T, Osuga K, Yoshimatsu R, et al. Development of a portable training tool for simulating visceral angiographic procedures for beginners. Cardiovascular and interventional radiology 2009; 32:412-6. DOI: 10.1007/s00270-009-9519-5
[10] Aggarwal R, Black SA, Hance JR, et al. Virtual reality simulation training can improve inexperienced surgeons' endovascular skills. Eur J Vasc Endovasc Surg 2006; 31:588-93. DOI: 10.1016/j.ejvs.2005.11.009
[11] Shibata E, Takao H, Amemiya S, et al. Embolization of visceral arterial aneurysms: Simulation with 3D-printed models. Vascular 2020; 28:259-66. DOI: 10.1177/1708538119900834
[12] Kaneko N, Mashiko T, Ohnishi T, et al. Manufacture of patient-specific vascular replicas for endovascular simulation using fast, low-cost method. Sci Rep 2016; 6:39168. DOI: 10.1038/srep39168
[13] Sun Z. Clinical Applications of Patient-Specific 3D Printed Models in Cardiovascular Disease: Current Status and Future Directions. Biomolecules 2020; 10. DOI: 10.3390/biom10111577
[14] Waqas M, Mokin M, Lim J, et al. Design and Physical Properties of 3-Dimensional Printed Models Used for Neurointervention: A Systematic Review of the Literature. Neurosurgery 2020; 87:E445-E53. DOI: 10.1093/neuros/nyaa134
[15] Kalejs M, von Segesser LK. Rapid prototyping of compliant human aortic roots for assessment of valved stents. Interact Cardiovasc Thorac Surg 2009; 8:182-6. DOI: 10.1510/icvts.2008.194134
[16] Mitsouras D, Liacouras P, Imanzadeh A, et al. Medical 3D Printing for the Radiologist. Radiographics 2015; 35:1965-88. DOI: 10.1148/rg.2015140320
[17] Coles-Black J, Bolton D, Chuen J. Accessing 3D Printed Vascular Phantoms for Procedural Simulation. Front Surg 2020; 7:626212. DOI: 10.3389/fsurg.2020.626212
[18] Kaufmann R, Zech CJ, Takes M, et al. Vascular 3D Printing with a Novel Biological Tissue Mimicking Resin for Patient-Specific Procedure Simulations in Interventional Radiology: a Feasibility Study. J Digit Imaging 2022; 35:9-20. DOI: 10.1007/s10278-021-00553-z
[19] Kaufmann R, Zech CJ, Deutschmann M, et al. Endovascular embolization techniques in acute thoracic and abdominal bleedings can be technically reproduced and trained in a standardized simulation setting using SLA 3D printing: a 1-year single-center study. Insights Imaging 2022; 13:72. DOI: 10.1186/s13244-022-01206-7

[20] Caldwell RA, Woodell JE, Ho SP, et al. In vitro evaluation of phosphonylated low-density polyethylene for vascular applications. J Biomed Mater Res 2002; 62:514-24. DOI: 10.1002/jbm.10249
[21] Chueh JY, Wakhloo AK, Gounis MJ. Neurovascular modeling: small-batch manufacturing of silicone vascular replicas. AJNR Am J Neuroradiol 2009; 30:1159-64. DOI: 10.3174/ajnr.A1543
[22] Karimi A, Navidbakhsh M, Shojaei A, et al. Measurement of the uniaxial mechanical properties of healthy and atherosclerotic human coronary arteries. Mater Sci Eng C Mater Biol Appl 2013; 33:2550-4. DOI: 10.1016/j.msec.2013.02.016
[23] Hasegawa H, Kanai H, Hoshimiya N, et al. Accuracy evaluation in the measurement of a small change in the thickness of arterial walls and the measurement of elasticity of the human carotid artery. Japanese Journal of Applied Physics Part 1-Regular Papers Short Notes & Review Papers 1998; 37:3101-5. DOI: Doi 10.1143/Jjap.37.3101
[24] Chen P-H, Zhang J, Tabaczynski J, et al. Use of patient specific 3D printed (3DP) neurovascular phantoms for mechanical assessment of devices used in image guided minimally invasive procedures. Presented at Medical Imaging 2018: Imaging Informatics for Healthcare, Research, and Applications2018.
[25] Reddy AS, Liu Y, Cockrum J, et al. Construction of a comprehensive endovascular test bed for research and device development in mechanical thrombectomy in stroke. Journal of neurosurgery 2020; 134:1190-7. DOI: 10.3171/2020.1.JNS192732

Figure Legends

Fig 1. Resin and porcine artery plates.

The left panel shows the Flexible 80A resin plates created by Form 3L using the desktop three-dimensional printer. The right panel shows the porcine artery plates created by excising the abdominal aorta immediately postmortem. The white arrow indicates the artery plates; the white arrowhead indicates the resin plate.

Fig 2. Unidirectional tensile test (a) and Tack test (b)

a. The left panel shows the tensile test of the resin. The resin plates were set and pulled by the machine. The right panel shows the tensile test of porcine artery plates.
b. Tack test of the resin surface toward polyethylene (PE) plate, the same material with the catheter tip, was evaluated by using the tensile-compressive mechanical tester. The white arrow indicates the resin plate; the white arrowhead indicates the PE plate.

Fig 3. General characteristics of Flexible 80A resin

a. Unidirectional tensile test: In the comparison among five resin groups (curing times of 0, 1, 3, 5, and 10 min) using Tukey's test, significant differences were observed in elastic modulus (E) between the 0-min and 5- and 10-min curing time groups ($P<0.05$). In the comparison using Dunnett's test with porcine arteries as control, there were significant

differences in E between the porcine arteries and resin plates at each curing time ($P<0.05$). resin: n=7, porcine arteries: n =6

b. Tack test: In the comparison among three groups (curing times of 0, 1, and 10min) and the artery group using Tukey's test, significant differences were observed in the adhesive stress (σ_A, kPa) and energy (Γ_A, MJ/m^2) between all groups ($P<0.05$), except for adhesive energy between artery and 10-min resin groups. The adhesive strength of the artery was the lowest. The adhesive strength and energy of uncured resin were higher than those of cured resin ($P<0.05$). The adhesive strength and energy of the 10-min cured resin were lower than those of the 1-min cured resin. resin: n=6, artery: n=6

※ P values of <0.05 indicate statistical significance (denoted with *, $P\leq0.05$; **, $P\leq0.001$), and multiple comparisons (Dunnett's and Tukey's tests) were performed with Bonferroni correction. n.s. = not significant

Fig 4. Characteristics of the silicone-coated resin

Friction test: The kinetic frictional coefficient (μ_k) of the inner surface of the porcine artery and silicone-coated resin in saline or air are shown. In the comparison using Dunnett's test with arteries as control, there were no significant differences in μ_k between the porcine arteries and silicone-coated resins with coating durations of 2 and 3 s in air and between the porcine arteries and silicone-coated resins with coating durations of 2, 3, and 4 s in saline solution. In

the comparison using Dunnett's test with the arteries as control, there were significant differences between the porcine arteries and silicone-coated resins with coating durations of 1, 4, and 5 s in air and between the porcine arteries and silicone-coated resins with coating durations of 1 and 5 s in saline solution ($P<0.001$). A total of 12 resin plates and one artery plate were used for each silicone application time (0-5s) in each condition (air/saline).

※ P values of <0.05 indicate statistical significance (denoted with *, $P\leq0.05$; **, $P\leq0.001$), and multiple comparisons (Dunnett's and Tukey's tests) were performed with Bonferroni correction.

n.s. = not significant.

Video 1. Interventional radiology (IR) simulation using transparent flexible vascular models

This video shows IR simulation using this vascular model of the normal celiac artery of a patient. A sheath (not shown in the video) is inserted into the vascular model, and a catheter is inserted through the sheath to manually manipulate the catheter. The 4Fr catheter can be visualized easily, with the catheter being manipulated satisfactorily. The catheter tip is inserted into the splenic artery.

Fig E1. Transparent flexible vascular models for interventional radiology (IR) simulation

a. The concepts for creating patient-specific hollow vascular models for IR simulation using

desktop three-dimensional (3D) printer. Digital Imaging and Communications in Medicine images of 3D computed tomographic angiography were converted to Standard Triangulated Language (STL) files after artery segmentation from computed tomography (CT) data. The hollow feature of the model was created using computer-aided design software. After output of the 3D data to the printing software, a hollow vessel model was prepared using a desktop 3D printer with flexible and transparent materials.

b. The left panel shows transparent and flexible patient-specific hollow vascular models printed using flexible resin (Flexible 80A) using the CT data of each patient (left: normal celiac artery, middle: renal artery arteriovenous malformation, right: renal artery aneurysm). The middle panel shows the flexibility of the models of the normal celiac artery of a patient. The aorta is easily compressed with two fingers. The right panel, including two images, shows IR simulation using this vascular model of a patient's right renal artery arteriovenous malformation. The guiding catheter and a stiff guidewire can be visualized easily (left-side image: before simulation, right-side image: catheter tip in the branch), and the right-side image shows that the introduction of a stiff guidewire and catheter into a branch, such as the renal artery, deforms the model (black arrow) similar to the deformation of a human artery, demonstrating the inferiority of the rigid model.

Fig E2. Friction test with a translational friction tester (a) for the artery (b) and silicone-coated resin.

a. The illustration shoes a translational friction tester. This machine has a pendulum seesaw at the center, which is leveled with a counterweight in front of the load cell. The alumina sphere, as a counter material, comes in contact with the sample (resin or artery), and the normal load is placed on the alumina sphere, leading to the movement of the translational reciprocator.
b. Friction test for the arterial plate is shown. The white arrows indicate the arterial plates; the black arrow indicates the alumina ball.

Fig E3. Ultraviolet-visible light (UV-Vis) absorption spectroscopy: The visible light transmittance (*T*, %, 400–700 nm) of the resin with curing times of 0, 1, 3, 5, and 10 min is shown.

Fig E4. The thickness of the silicone coating with coating durations of 1, 2, 3, 4, and 5 s (a) and the relationship between μ_k and the thickness of the silicone coating (b).

a. The thickness of the silicone-coated resin according to the silicone application time (1, 2, 3, 4, and 5 s) is show in the left figure. The thickness of the silicone-coated resin using Tukey's test; the thickness increased significantly with increased spraying time ($P<0.05$);

however, it plateaued at 4 and 5 s. The blue graph shows the silicone application duration of 2 or 3 s for friction test results close to the porcine arteries, and the red graph shows the silicone application duration of 1, 4, or 5 s. The right upper panel shows the topological map of the silicone coating on the resin plate. The right down panel shows the boundary of silicone-coating on the resin plate with a 3D laser microscope. The left flat region and right rough region denote the silicone coating layer and bare resin surface, The flat lesion (area) indicated by the arrow shows silicone coating. respectively.

※ P values of <0.05 indicate statistical significance (denoted with *, P≤0.05; **, P≤0.001), and multiple comparisons (Dunnett's and Tukey's tests) were performed with Bonferroni correction. n.s. = not significant.

b. The thickness of the silicone coating is plotted on the horizontal axis; t is the silicone application time (0, 1, 2, 3, 4, and 5 s). The red line indicates μ_k of the artery, the blue circle indicates μ_k and the silicone thickness in saline solution, and the green circle indicates μ_k and the silicone thickness in air, in the friction test results. The thickness of the silicone layer (1.6–2 μm) at 2 and 3 s exhibited similar μ_k as the porcine artery. The frictional force increased by increasing the thickness of the silicone coating over about 2.4 μm. ※ t = inset time is silicone-spraying duration

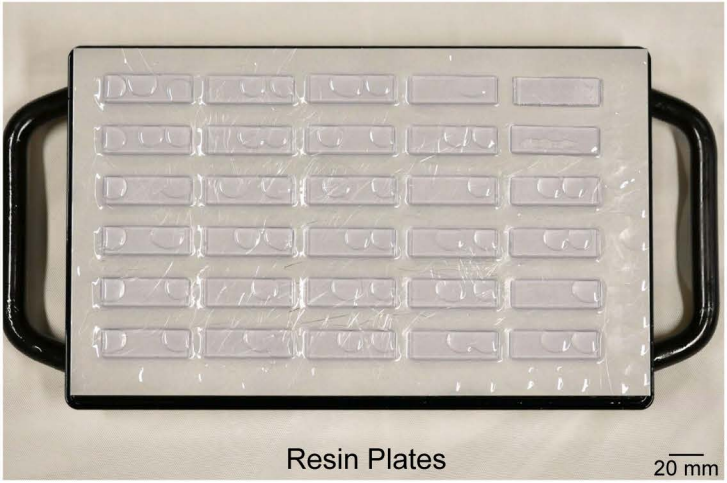
Table 1. Characteristics of Flexible80A resin and silicone-coated resin

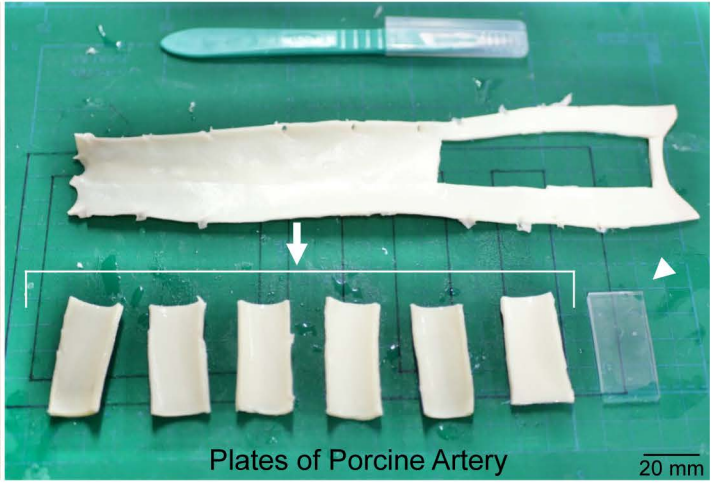
	Curing time [min]	**Silicone coating** [s]	**Silicone thickness** [μm]	**Tensile test** [MPa]	**Adhesive strength** [kPa]	**Adhesive energy** [J/m^2]	**Frictional coefficient**
Artery	−	−	−	0.20 (±0.04)	1.57 (±0.91)	0.122 (±0.06)	0.055 (±0.025)
Resin	0	−	−	5.50 (±1.15)	29.84 (±0.25)	1.36 (±0.03)	−
	1	−	−	8.53 (±2.37)	6.50 (±0.44)	0.35 (±0.02)	−
	5	−	−	9.50 (±1.43)	−	−	−
	10	−	−	8.89 (±1.45)	2.57 (±0.53)	0.06 (±0.02)	−
	3	0	0	8.63 (±1.12)	−	−	1.060 (±0.043)
	↓	1	1.18 (±0.07)	−	−	−	0.242 (±0.047)

	↓	2	1.63	−	−	−	0.038
			(±0.02)				(±0.018)
	↓	3	1.94	−	−	−	0.034
			(±0.05)				(±0.007)
	↓	4	2.41	−	−	−	0.053
			(±0.10)				(±0.009)
	↓	5	2.47	−	−	−	0.104
			(±0.06)				(±0.010)

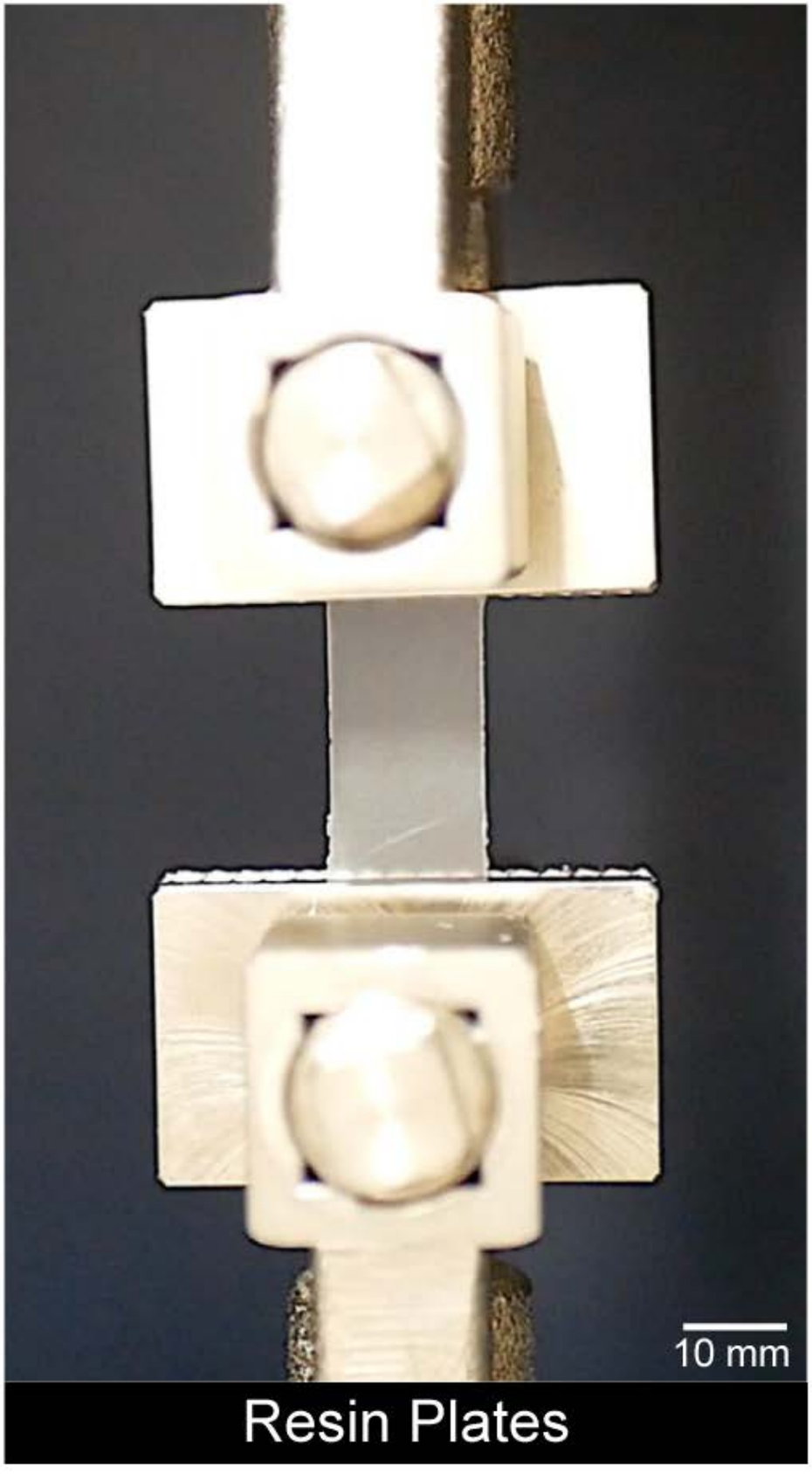
Note – All downward arrows indicate the 3-min curing time

Frictional coefficient ＝ Kinetic frictional coefficient (μ_k) in saline solution


Resin Plates
20 mm


Plates of Porcine Artery
20 mm

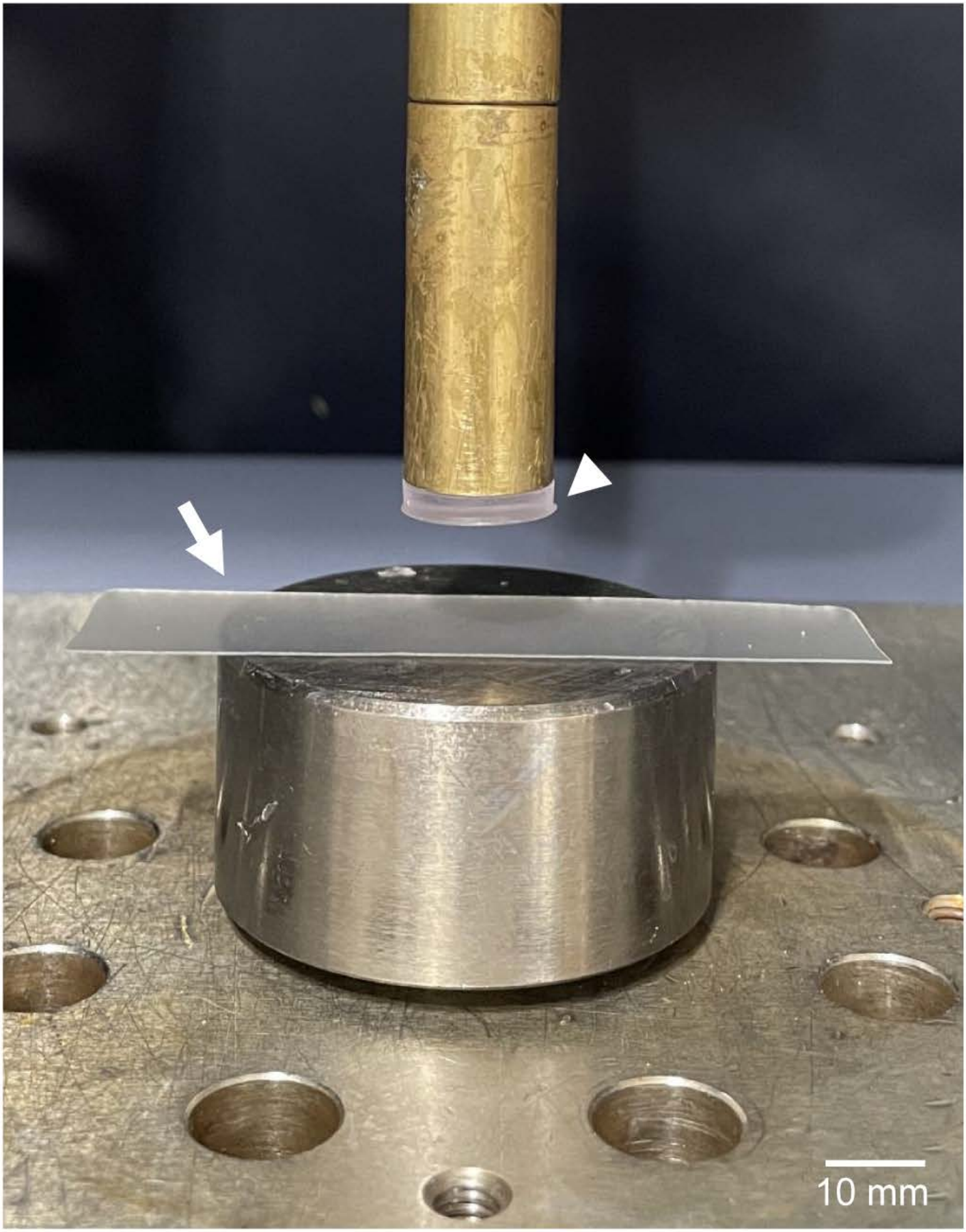
Tensile Test



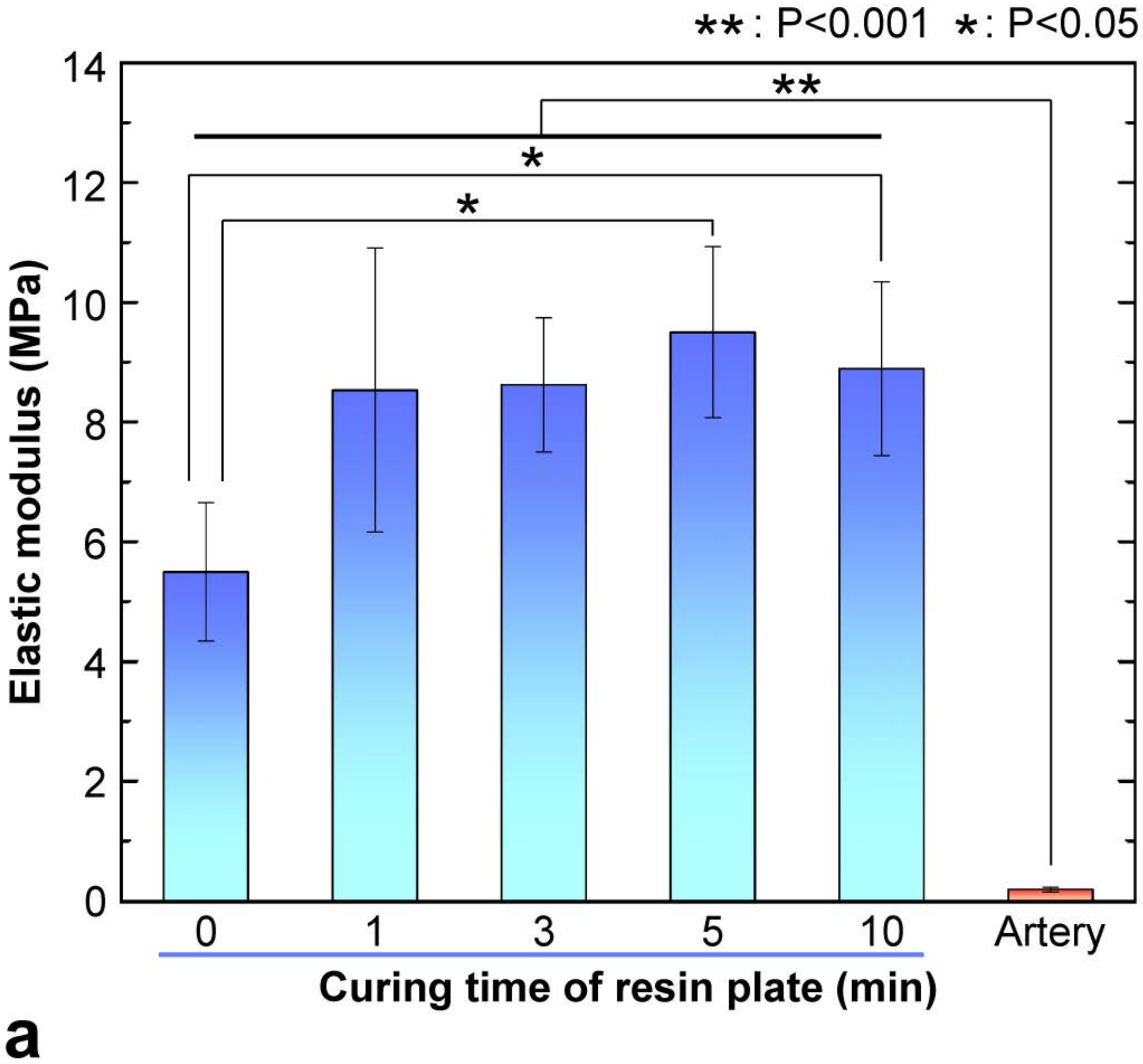


a

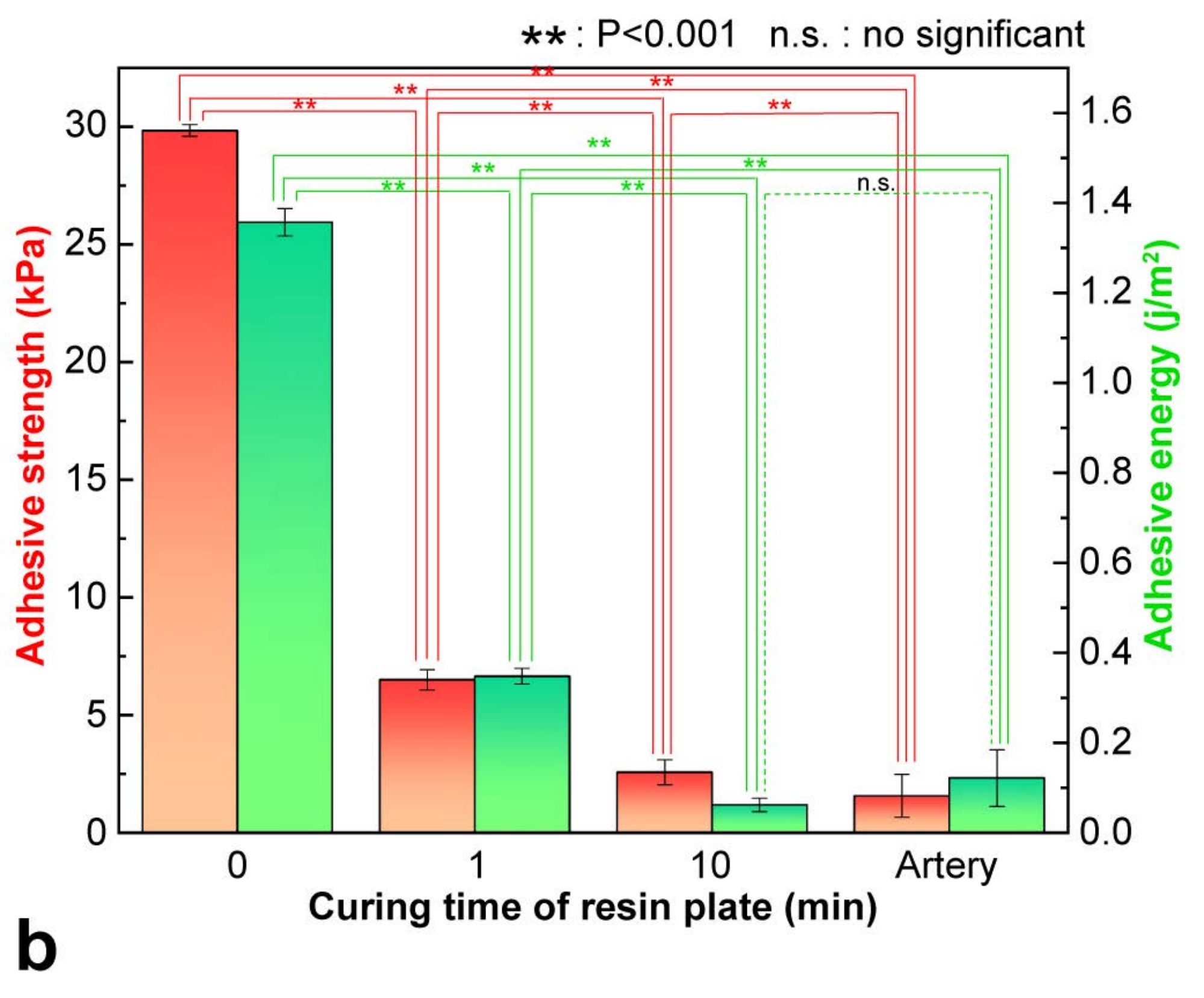
Tack test

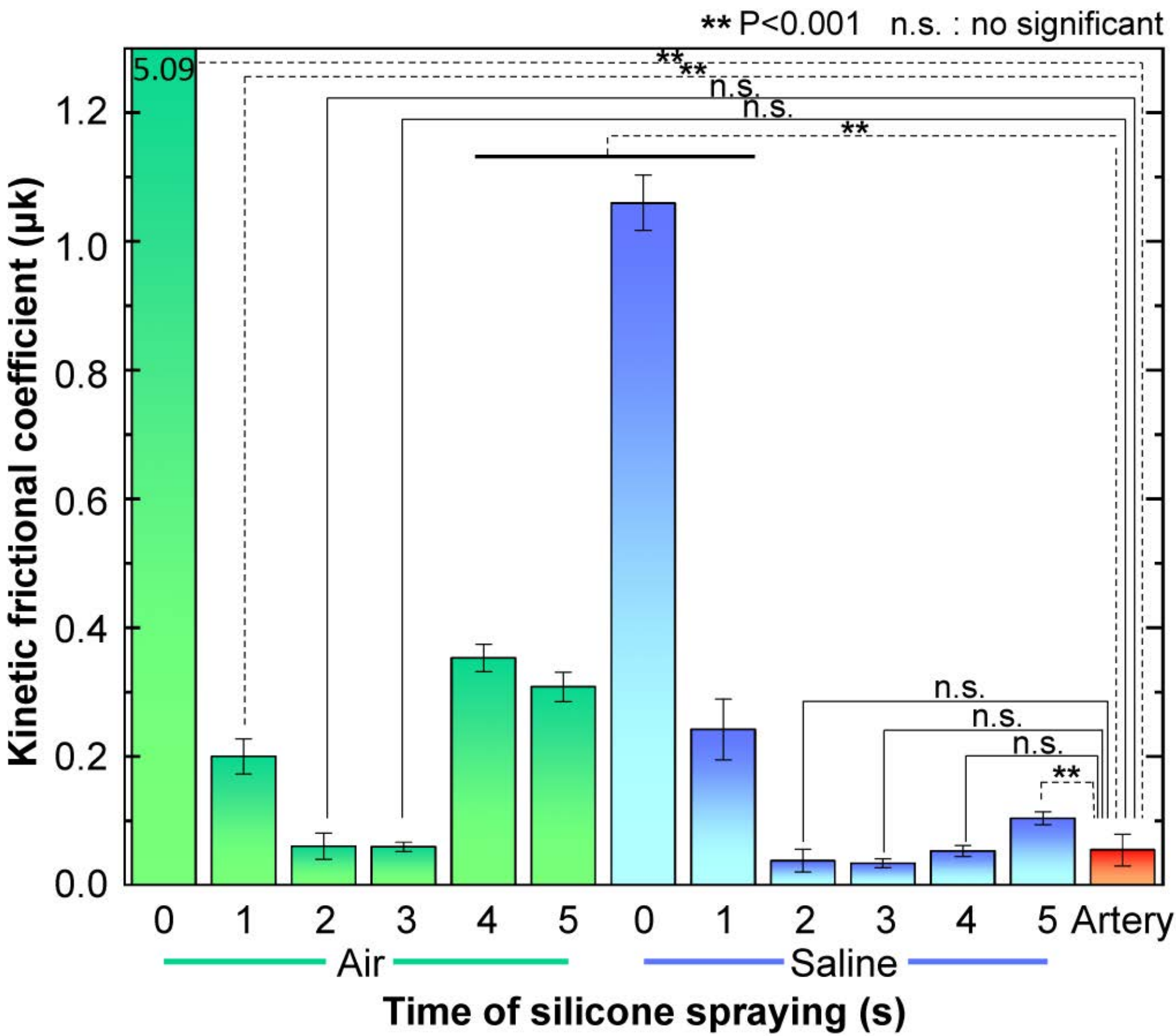


b


**: P<0.001 *: P<0.05
14
12
10
8
6
4
2
0
Elastic modulus (MPa)
**
*
*
0
1
3
5
10
Artery
Curing time of resin plate (min)

a


**: P<0.001 n.s. : no significant
Adhesive strength (kPa)
Adhesive energy (j/m²)
Curing time of resin plate (min)
0
1
10
Artery
n.s.
b


** P<0.001 n.s. : no significant
5.09
**
**
n.s.
n.s.
**
n.s.
n.s.
n.s.
**
Kinetic frictional coefficient (μk)
0.0
0.2
0.4
0.6
0.8
1.0
1.2
0 1 2 3 4 5 0 1 2 3 4 5 Artery
Air
Saline
Time of silicone spraying (s)